Journal of Science: Advanced Materials and Devices 5 (2020) 527–534

Contents lists available at ScienceDirect

Journal of Science: Advanced Materials and Devices

journal homepage: www.elsevier.com/locate/jsamd

Original Article

Fracture toughness enhancement of yttria-stabilized tetragonal zirconia polycrystalline ceramics through magnesia-partially stabilized zirconia addition

Bilal Soylemez [a], Ercan Sener [a], Arife Yurdakul [a, b], Hilmi Yurdakul [a, c, *, 1]

[a] Department of Metallurgical and Materials Engineering, Alanya Alaaddin Keykubat University, Alanya-Antalya, Turkey
[b] Department of Hand Arts, Kutahya Vocational School of Fine Arts, Kutahya Dumlupinar University, Kutahya, Turkey
[c] Department of Mechanical Engineering, Kutahya Dumlupinar University, Kutahya, Turkey

ARTICLE INFO

Article history:
Received 23 May 2020
Received in revised form
22 August 2020
Accepted 6 September 2020
Available online 9 September 2020

Keywords:
Biomaterials
Fracture toughness
Mechanical properties
8 Mg-PSZ
3Y-TZP
Zirconia

ABSTRACT

In this work, for the first time, we report a novel method on the fracture toughness enhancement of 3 mol % yttria-stabilized tetragonal zirconia polycrystalline (3Y-TZP) ceramics through the incorporation of 8 mol % magnesia-partially stabilized zirconia (8 Mg-PSZ) powders having high fracture toughness. Highly densified composites (x3Y-TZP/y8Mg-PSZ; where x and y vary between 0.25 and 0.75 wt. %) were obtained with a relative density over 99% by pressureless sintering. Relative density, Vickers hardness (HV) and indentation fracture toughness (K_{Ic}) were significantly improved by sintering temperature and dwell-time increment. Specifically, HV and K_{Ic} values of 0.5(3Y-TZP)/0.5(8 Mg-PSZ) composite sintered at 1500°C-2h were increased by 7% and 30%, respectively, compared to that of 3Y-TZP. Sintered bodies consisted of c-ZrO_2, t-ZrO_2 and m-ZrO_2 phases without any new phase formation. m-ZrO_2/c-ZrO_2+t-ZrO_2 volumetric phase ratios changed with the increase of sintering temperature and time. Stress-induced t-ZrO_2 → m-ZrO_2 phase transformation within c-ZrO_2 grains in 8 Mg-PSZ was the main mechanism for toughness enhancement. Energy absorbing mechanisms, e.g., crack-bridging, crack-deflection and crack branching were also found to contribute the blunting of cracks. It is thought that our approach presented herein can be considered not only fracture toughness enhancement but also other properties in various materials for functional and structural purposes.

© 2020 The Authors. Publishing services by Elsevier B.V. on behalf of Vietnam National University, Hanoi.
This is an open access article under the CC BY license (http://creativecommons.org/licenses/by/4.0/).

1. Introduction

Due to its high flexural strength, superior biocompatibility and good chemical resistance, zirconium oxide [zirconia (ZrO_2)] has been widely used so far for different functional and structural purposes e.g., biomaterials: dental, hip and knee implants, cutting tools, bearings and bushings [1]. ZrO_2 has three main crystallographic polymorphs: monoclinic (m-ZrO_2), tetragonal (t-ZrO_2) and cubic (c-ZrO_2) [2]. Metallic oxides such as yttrium oxide (Y_2O_3) and magnesium oxide (MgO) are generally utilized to stabilize the t-ZrO_2 and c-ZrO_2 phases at room temperature [2].

Especially, when 3 mol % Y_2O_3 enters to the t-ZrO_2 crystal structure, the resulting product at room temperature is called as yttrium stabilized tetragonal zirconia polycrystalline (3Y-TZP) ceramic [3]. In addition, 3Y-TZPs are the most popular material used in the bio-based ceramics to improve the mechanical properties [1]. They exhibit high flexural strength between 900 and 1100 MPa; however, with low or moderate fracture toughness that is around 5.0 MPa $m^{1/2}$ [4]. Based on the detailed literature survey, the stress-induced t-ZrO_2 → m-ZrO_2 phase transformation plays a key role to gain high fracture toughness and strength by causing a significant volume change (~4–5%), resulting in compression at the vicinity of advancing crack [5]. Thus, transformation-toughening occurs in the 3Y-TZP ceramics to further stop the cracks [5]. However, these excellent mechanical properties of the 3Y-TZPs suffer from a low temperature (150–400 °C) degradation phenomenon in the presence of water or water environment due to the enhanced t-ZrO_2 → m-ZrO_2 phase transformation [6].

* Corresponding author. Alanya Alaaddin Keykubat University, Rafet Kayis Faculty of Engineering, Department of Metallurgical and Materials Engineering, Kestel Campus, University Street, 07450, Alanya-Antalya, Turkey. Fax: +90 242 510 6124.
E-mail addresses: hilmi.yurdakul@alanya.edu.tr, hilmi.yurdakul@dpu.edu.tr (H. Yurdakul).

Peer review under responsibility of Vietnam National University, Hanoi.

[1] Permanent address: Kutahya Dumlupinar University, Faculty of Engineering, Department of Mechanical Engineering, Evliya Celebi Campus, Tavsanli Road 10. Km, 43100, Kutahya, Turkey. Fax: +90 274 265 2066.

https://doi.org/10.1016/j.jsamd.2020.09.003
2468-2179/© 2020 The Authors. Publishing services by Elsevier B.V. on behalf of Vietnam National University, Hanoi. This is an open access article under the CC BY license (http://creativecommons.org/licenses/by/4.0/).

MgO is another commonly used stabilizing material that its amount ranges between 8 and 10 mol % in the starting batches [7,8]. Magnesia partially stabilized zirconia (Mg-PSZ) ceramics are thus obtained by introducing Mg^{2+} cations into the c-ZrO_2 and/or t-ZrO_2 lattices [7,8]. Here, unlike the TZP structure, PSZ usually consists of two or more ZrO_2 phases [7,8]. More specifically, the large polygonal-shaped c-ZrO_2 phase, lenticular-type formed t-ZrO_2 precipitates within the c-ZrO_2 grains, and spherical m-ZrO_2 phase along the grain boundaries are uniquely observed in the Mg-PSZ microstructures after sintering [7,8]. In addition, Mg-PSZ ceramics exhibit quite good mechanical properties due to the transformation-toughening mechanism just like that of the Y-TZP counterparts. So, the Mg-PSZ ceramics have high fracture toughness (between 8 and 15 MPa $m^{1/2}$) and good flexural strength (around 450–820 MPa). They also show the outstanding high temperature properties e.g., creep and thermal shock resistance, and hence are generally considered as a structural ceramic as well [9–12]. Moreover, the low temperature degradation of Mg-PSZ ceramics is more stable than that of Y-TZPs [9]. Therefore, the Mg-PSZs have been alternatively experienced for possible biomedical applications [14].

When studies intended for fracture toughness improvement of 3Y-TZP ceramics were examined, it was firstly noteworthy that Y_2O_3 was used in less than 3% mole (e.g. 1.5% and 2 mol %) as stabilizing agent [15,16]. Afterwards, the fracture toughness of 3Y-TZP was tried to be developed by adding many different secondary reinforcement materials such as especially Al_2O_3, carbon nanotubes (CNTs), graphene etc. [17–19]. In addition, the effects of different new sintering techniques such as spark plasma sintering (SPS), microwave sintering and two-step sintering were reported on the mechanical properties enhancement of 3Y-TZP ceramics [20]. Although these researches have made very important contributions scientifically, it can be evaluated as known drawbacks that complete dense bodies are not obtained, secondary phases cannot be fully distributed within the 3Y-TZP, and the proposed new sintering techniques are not suitable for industrialization. Therefore, more practical, industrial and feasible new approaches are still needed to improve the fracture toughness of 3Y-TZPs.

In this study, it is aimed, for the first time in the literature, to increase the fracture toughness of 3Y-TZP based sintered bodies

Table 1
Elastic modulus (E) of each recipe.

Sample Name	E (GPa)
3Y-TZP	210.00
0.75(3Y-TZP)/0.25(8 Mg-PSZ)	205.27
0.5(3Y-TZP)/0.5(8 Mg-PSZ)	200.69
0.25(3Y-TZP)/0.75(8 Mg-PSZ)	196.28
8 Mg-PSZ	192.00

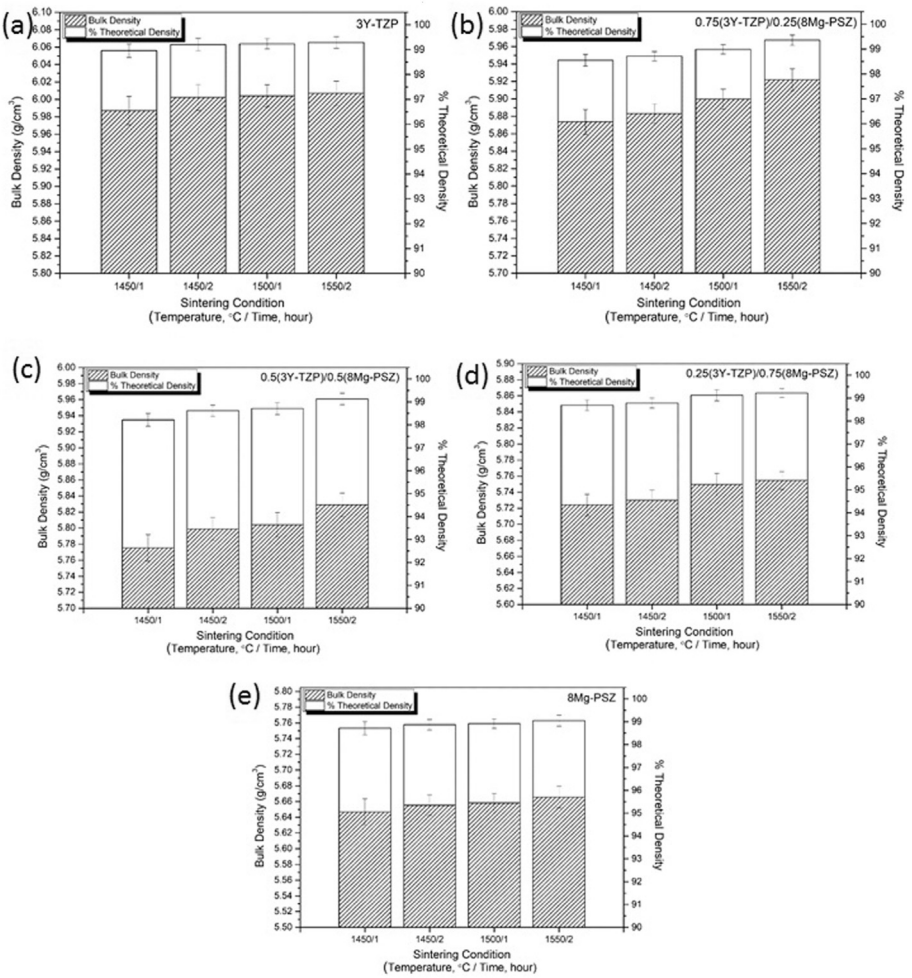

Fig. 1. The bulk and % relative density results of (a) 3Y-TZP, (b) 0.75(3Y-TZP)/0.25(8 Mg-PSZ), (c) 0.5(3Y-TZP)/0.5(8 Mg-PSZ), (d) 0.25(3Y-TZP)/0.75(8 Mg-PSZ), and (e) 8 Mg-PSZ specimens sintered at 1450°C–1500 °C for 1–2 h.

through the combination of 3Y-TZP powders with 8 Mg-PSZ powders having high fracture toughness. For this purpose, the effects of sintering temperature and dwell-time were examined on the production of designed zirconia composites. Physical, mechanical and microstructural investigations of sintered bodies were carried out in detail. Possible mechanisms on the fracture toughness enhancement are also discussed.

2. Experimental

3Y-TZP (Admat Co., India) and 8 Mg-PSZ (Admat Co., India) commercially available zirconia powders were utilized here as starting raw materials. The 3Y-TZP, 0.75(3Y-TZP)/0.25(8 Mg-PSZ), 0.5(3Y-TZP)/0.5(8 Mg-PSZ), 0.25(3Y-TZP)/0.75(8 Mg-PSZ) and 8 Mg-PSZ recipes were prepared considering weight % ratios by using dry-ball milling during 24 h. After homogenization, the powder mixtures were sieved by 180 μm sized sieve to break up weakly bonded agglomerates. Then, the powders were pre-shaped in circular stainless-steel die by a uniaxial press under 30 MPa pressure. Following, cold isostatic pressing (CIP) was performed by 250 MPa to achieve high green density compacts. The binder burn-out process was applied to CIPed samples at 700 °C for 2 h with 0.8 °C/min heating speed to control the removal of the organics from green bodies. Afterwards, the specimens were densified by pressureless sintering route in ambient atmosphere. In sintering process, the maximum temperature was reached by a heating rate of 1.5 °C/min, and then held at 1450–1500 °C for 1–2 h before cooling to room temperature with 10 °C/min speed.

The relative densities of sintered samples were determined by Archimedes' method [21]. In this step, theoretical density of each designed recipe was calculated according to rule-of-mixtures [22]. Therefore, the theoretical densities of 3Y-TZP and 8 Mg-PSZ powders were respectively taken into account as 6.10 g cm^{-3} and 5.80 g cm^{-3} in the calculations [23,24]. The crystalline phase contents of the sintered specimens were determined by X-ray diffraction analysis (Rigaku MiniFlex 600) with a scanning speed of 1°/min between $2\theta = 5–80°$ scanning range. The Cu-K_α source was also used at 40 kV and 10 mA during XRD analysis. The phase ratio of m-ZrO_2 to t-ZrO_2 plus c-ZrO_2 phases was obtained from the formulation developed by Toroya et al. [25], depending on the specific crystallographic planes for related zirconia phases. Vickers hardness and indentation fracture toughness tests were performed on the polished surfaces of sintered samples to clarify the mechanical properties. Tests were carried out by Vickers hardness tester (Emco Test M1C 010) with a dwell time of 15 s and applying 294 N indentation load. Please note that the samples were also subjected to low loads, but no sufficient cracking was encountered in the indent's corners. Moreover, distance between the indentations was retained constant to prevent their overlapping effect [26]. At least twenty-five indents were obtained from each sample to evaluate the mean values. Thus, Vickers hardness was calculated based on the following equation [27,28].

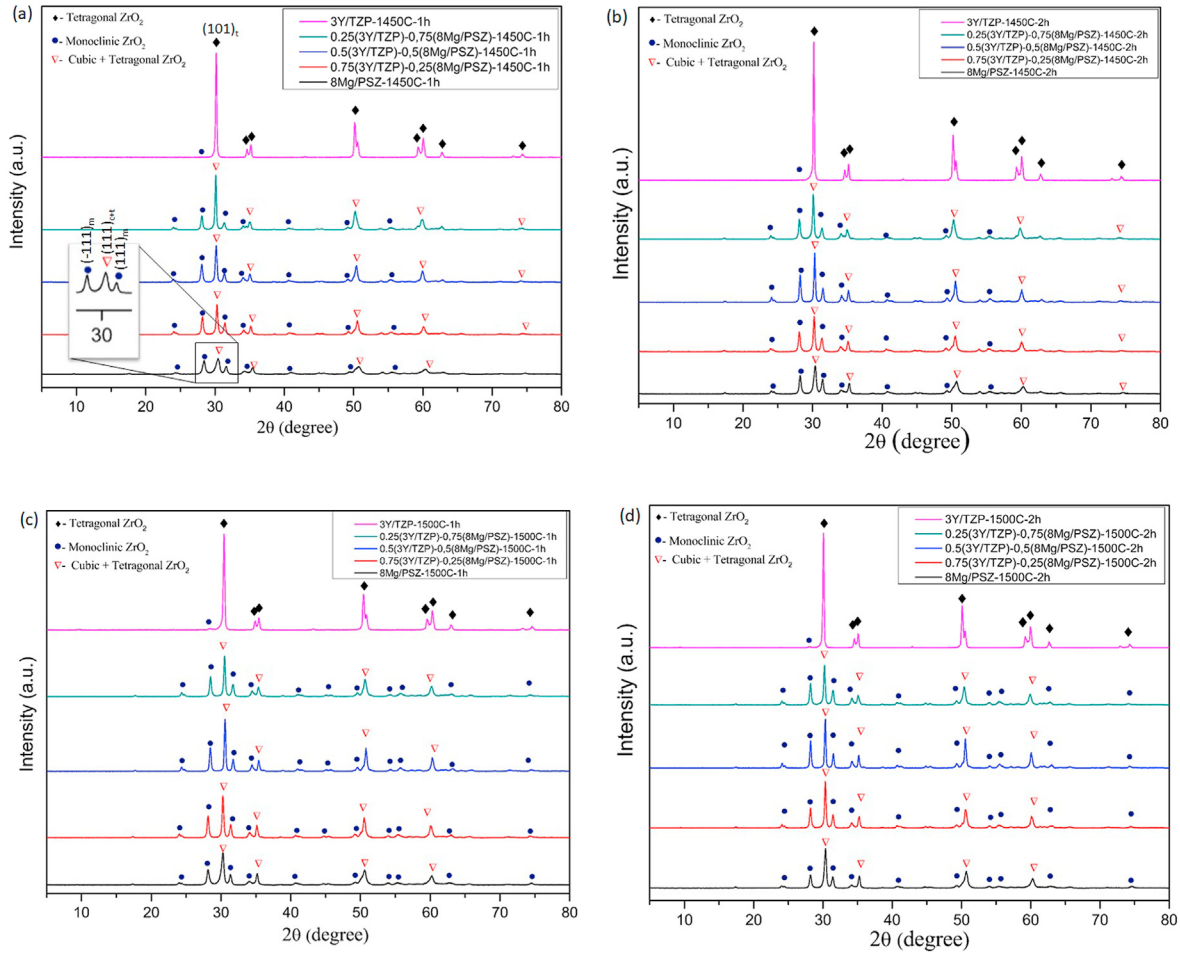

Fig. 2. The XRD analysis results of reference (3Y-TZP and 8 Mg-PSZ) and composite (x3Y-TZP/y8Mg-PSZ; x and y = 0.25–0.75 wt. %) bodies sintered at (a) 1450°C-1h, (b) 1450°C-2h, (c) 1500°C-1h and (d) 1500°C-2h.

$$H = 1.8544\frac{P}{d^2} \quad (1)$$

In Eq. (1), P and d terms are called as applied load and indent diagonals, respectively. The indent diagonals were precisely measured by means of optical microscopy. Niihara et al.'s reports [27,28] were considered to calculate the indentation fracture toughness of sintered samples, since the cracks were Palmqvist-type rather than radial-median ones in the ceramics [29,30]. Accordingly, the Eq. (2) was utilized to determine the fracture toughness values.

$$\left(\frac{K_{Ic}\phi}{Ha^{1/2}}\right)*\left(\frac{H}{E\phi}\right)^{2/5} = 0.035\left(\frac{c}{a}\right)^{-1/2} \text{for } 0.25 < 1/\,a < 2.5 \quad (2)$$

Herein, K_{Ic} is the fracture toughness, φ the geometric constant ≅ 3, H the hardness, the a equivalent to d/2, E the Young's modulus, and the c the crack length. Additionally, E values of each recipe were evaluated by the rule-of-mixtures [22]. At this point, Young's modulus of 8 Mg-PSZ and 3Y-TZP were taken as 192 GPa and 210 GPa, respectively [12,31]. The calculated E values of each recipe were also presented in Table 1.

Lastly, the microstructural observations of sintered samples were examined by scanning electron microscopy (SEM, Zeiss Supra 50VP) attached with an energy dispersive X-ray spectroscopy (EDXS). During SEM analysis, the microscope was operated at 20.00 kV, and back scattered electron imaging (BSEI) was preferred to distinguish the phases in variable pressure (VP) mode without coating. Furthermore, the samples were characterized by using a field emission gun (FEG) ultra-high resolution scanning electron microscope (UHR-SEM, FEI Nova Nano 650) to precisely investigate the microstructure features.

3. Results and discussion

Fig. 1(a–e) reveals the bulk and relative density results of 3Y-TZP, 0.75(3Y-TZP)/0.25(8 Mg-PSZ), 0.5(3Y-TZP)/0.5(8 Mg-PSZ), 0.25(3Y-TZP)/0.75(8 Mg-PSZ) and 8 Mg-PSZ coded samples that sintered at 1450 °C and 1500 °C for 1–2 h. Broadly speaking, the specimens were successfully densified up to ~99% of their theoretical densities (TD). Here, the increasing of sintering temperature and holding time gave rise to enhance the densification of samples during sintering. Especially, looking at the data in Fig. 1(a–e) in terms of as-received zirconia bodies (3Y-TZP and 8 Mg-PSZ) and their composite counterparts, the maximum relative density values (≥99%) were reached at 1500 °C and 2 h sintering conditions. More importantly, the results implied that the incorporation of different zirconia powders into each other could lead to easy sintering without any problems and deterioration on the samples by using pressureless sintering method. Considering the literature survey, 3.5 wt. % Mg-PSZ powders could be sintered up to ~95% maximum of relative density at 1670 °C [10]. In addition, 99.1% of TD was obtained at 1500 °C in Mg-PSZ and 1.7 mol % Y_2O_3-doped Mg-PSZ samples [11]. It was also known that 3Y-TZP powders exhibited very good sintering behavior between 1450 and 1500 °C [3]. At this point, our results are in agreement with those previously reported studies that related to as-received 3Y-TZP and 8 Mg-PSZ bodies [3–14].

To determine the crystalline phase contents, transformations and new formations after sintering, the XRD data was collected from all samples sintered at 1450 °C and 1500 °C for 1–2 h, and the results were presented in Fig. 2(a–d). The XRD patterns were also recorded from well-polished sample surfaces rather than that of powder XRD analysis, since t-ZrO_2 → m-ZrO_2 phase transformation can be strongly affected during the powder grinding step for sample preparation [32]. Thus, it was ensured to avoid from the misleading results. Additionally, volumetric phase ratios of m-ZrO_2 to t-ZrO_2+c-ZrO_2 for all designed compositions were quantitatively computed from {111} crystallographic X-ray peaks and summarized in Table 2. Accordingly, the 3Y-TZP sample was almost completely composed of t-ZrO_2 (98-015-7619) phase, while the Mg-PSZ sample was determined to contain m-ZrO_2 (98-008-9426) and t-ZrO_2 plus c-ZrO_2 (98-005-3998) phases [Fig. 2(a–d)] [33]. Here, please note that the $(101)_{t\text{-}ZrO2}$ and $(111)_{c\text{-}ZrO2}$ peaks were overlapped due to the similar lattice parameters of t-ZrO_2 and c-ZrO_2 phases [8]. Moreover, all zirconia phases (m-ZrO_2, t-ZrO_2 and c-ZrO_2) can be clearly discerned in the XRD patterns of 0.75(3Y-TZP)/0.25(8 Mg-PSZ), 0.5(3Y-TZP)/0.5(8 Mg-PSZ) and 0.25(3Y-TZP)/0.75(8 Mg-PSZ) composite samples [Fig. 2(a–d)]. Furthermore, when sintering temperature and dwell-time were increased, no new phase formation was detected rather than known zirconia polymorphs. However, X-ray peak intensities of the m-ZrO_2, t-ZrO_2 and c-ZrO_2 phases at $(\bar{1}11)_m$, $(111)_m$, $(101)_t$ and $(111)_c$ crystallographic planes significantly changed depending on rising sintering temperature and holding time [Fig. 2(a–d)]. This strongly implies the t-ZrO_2 → m-ZrO_2 and c-ZrO_2 → t-ZrO_2 phase transformations arising from the 3Y-TZP and Mg-PSZ sides during sintering [5,13,32].

Considering the results in Table 2, the volumetric phase amount of m-ZrO_2 slightly increased when the sintering time was raised from 1 to 2 h for both 1450 °C and 1500 °C. On the other hand, when the sintering temperature was increased from 1450 °C to 1500 °C, a significant reduction was generally determined in the amounts of m-ZrO_2. To some extent, this situation can be explained by ZrO_2–MgO and ZrO_2–Y_2O_3 phase equilibria diagrams, showing that more stable t-ZrO_2 and c-ZrO_2 phases can be formed at elevated temperatures [34,35]. Jiang et al. [10] reported that when the sintering temperature was just increased from 1600 °C to 1700 °C in Mg-PSZ ceramics, the m-ZrO_2 volumetric phase content drastically decreased from 80% to 5%. This is of paramount

Table 2
The volumetric phase ratios of m-ZrO_2 and t-ZrO_2+c-ZrO_2.

Sample	Sintering Temperature 1450 °C			Sintering Temperature 1500 °C		
	Sintering Time (h)	Tetragonal + Cubic Phase %	Monoclinic Phase %	Sintering Time (h)	Tetragonal + Cubic Phase %	Monoclinic Phase %
3Y-TZP	1	99.15 ± 1	0.85 ± 1	1	97.92 ± 1	2.08 ± 1
3Y-TZP	2	99.01 ± 1	0.99 ± 1	2	97.43 ± 1	2.57 ± 1
0.75(3Y-TZP)/0.25(8 Mg-PSZ)	1	66.68 ± 1	33.32 ± 1	1	53.26 ± 1	46.74 ± 1
0.75(3Y-TZP)/0.25(8 Mg-PSZ)	2	62.44 ± 1	37.56 ± 1	2	52.55 ± 1	47.45 ± 1
0.5(3Y-TZP)/0.5(8 Mg-PSZ)	1	50.88 ± 1	49.12 ± 1	1	51.64 ± 1	48.36 ± 1
0.5(3Y-TZP)/0.5(8 Mg-PSZ)	2	47.45 ± 1	52.55 ± 1	2	47.95 ± 1	52.05 ± 1
0.25(3Y-TZP)/0.75(8 Mg-PSZ)	1	44.46 ± 1	55.54 ± 1	1	51.41 ± 1	48.59 ± 1
0.25(3Y-TZP)/0.75(8 Mg-PSZ)	2	43.47 ± 1	56.53 ± 1	2	47.74 ± 1	52.26 ± 1
8 Mg-PSZ	1	35.78 ± 1	64.22 ± 1	1	54.56 ± 1	45.44 ± 1
8 Mg-PSZ	2	29.66 ± 1	70.34 ± 1	2	48.35 ± 1	44.65 ± 1

importance to understand the mechanical properties of ZrO_2-based materials [10,11].

Fig. 3(a and b) shows the Vickers hardness (HV) and indentation fracture toughness (K_{Ic}) results of as-received (3Y-TZP and 8 Mg-PSZ) and composite (0.75(3Y-TZP)/0.25(8 Mg-PSZ), 0.5(3Y-TZP)/0.5(8 Mg-PSZ), 0.25(3Y-TZP)/0.75(8 Mg-PSZ)) samples sintered at 1450°C–1500 °C for 1–2 h. In general, based on the as-received 3Y-TZP and 8 Mg-PSZ samples findings [Fig. 3(a and b)], the HV values of 3Y-TZP sintered bodies were measured as ~12.0–12.5 GPa and the K_{Ic} values were approximately around 5.5–6.0 MPa $m^{1/2}$, while the HV and K_{Ic} data of 8 Mg-PSZ samples were determined as ~10.0–11.0 GPa and ~7.0–8.5 MPa $m^{1/2}$, respectively. These results are quite compatible with the mechanical properties of sintered bodies with 3Y-TZP and 8 Mg-PSZ in the literature [3,4,9–13]. In addition, it was noteworthy that the K_{Ic} values increased; however, the HV values decreased linearly with the increase of sintering temperature and dwell-time. In other words, the K_{Ic} values of composite bodies increased significantly, whereas the HV values decreased simultaneously, as expected with the incorporation of 8 Mg-PSZ into the 3Y-TZP. More specifically, it could be expressed that the best mechanical properties were obtained at 1500°C-2h in terms of process parameters. In particular, for instance, the K_{Ic} and HV values of 0.5(3Y-TZP)/0.5(8 Mg-PSZ) composite sample were recorded as 7.59 ± 0.35 MPa $m^{1/2}$ and 10.98 ± 0.34 GPa, respectively. So, based on 1500°C-2h values, it was found that the fracture toughness of 0.5(3Y-TZP)/0.5(8 Mg-PSZ) composite sample increased by ~30% when compared to that of 3Y-TZP. Similarly, an increase of about 7% more than that of Mg-PSZ sample's hardness value was achieved in 0.5(3Y-TZP)/0.5(8 Mg-PSZ) composite due to addition of 3Y-TZP. This result clearly shows that the mechanical properties i.e., Vickers hardness and fracture toughness can be easily tailored in the composites formed by using 3Y-TZP and 8 Mg-PSZ together.

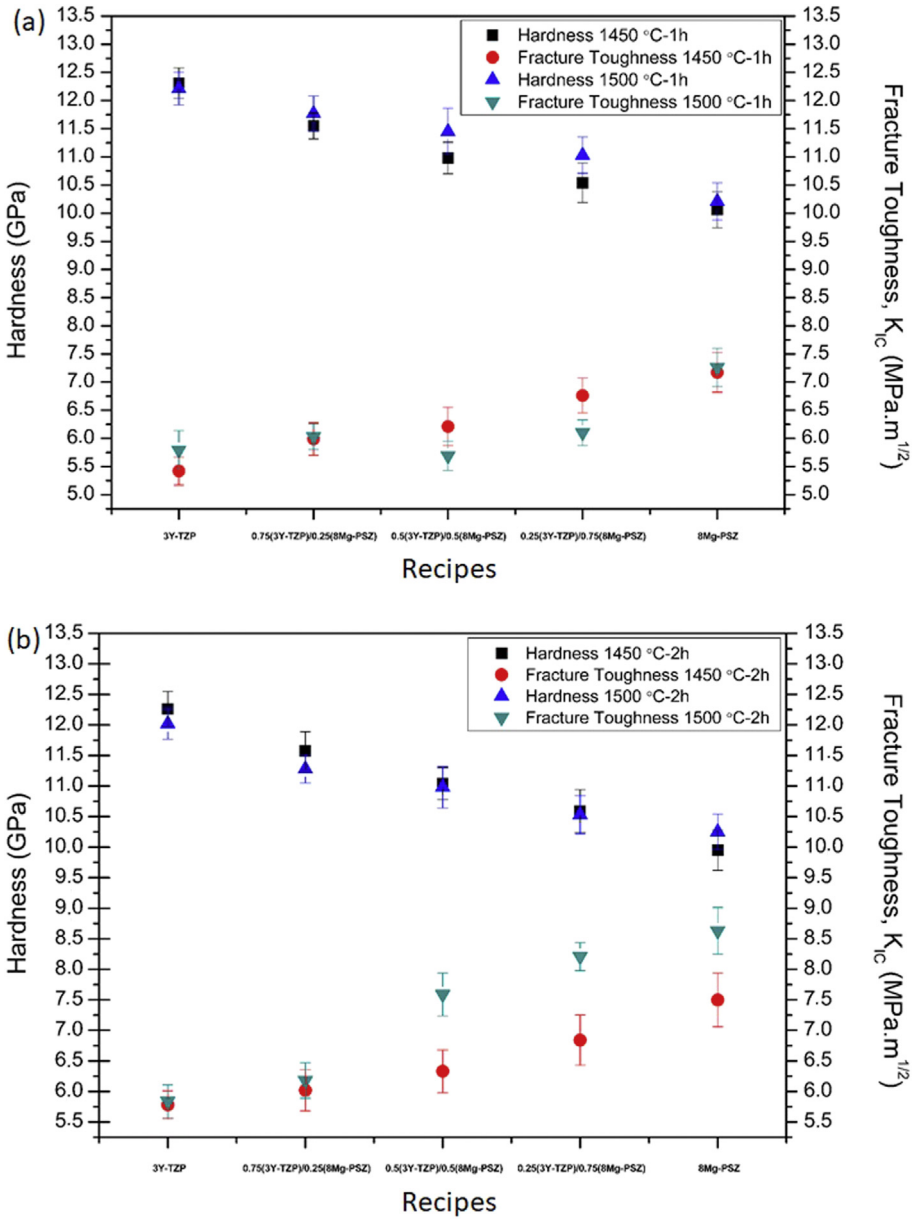

Fig. 3. The Vickers hardness and indentation fracture toughness values of reference (3Y-TZP and 8 Mg-PSZ) and composite (x3Y-TZP/y8Mg-PSZ; x and y = 0.25–0.75 wt. %) bodies sintered at (a) 1450°C–1500 °C/1 h and (b) 1450°C–1500 °C/2 h.

Here, transformation of precipitates developing in the form of ellipsoidal, disc, lens or small spheres in the c-ZrO_2 grains can be shown as the reason for increasing the indentation fracture toughness values with 8 Mg-PSZ addition [13]. The toughening mechanism was also reported to be related to stress-induced t-$ZrO_2 \rightarrow$ m-ZrO_2 phase transformation in 8 Mg-PSZ ceramics [36]. In addition, high fracture toughness was provided by means of transformable t-ZrO_2 precipitates that only occurred by suitable sintering conditions such as temperature and time as well as controlled cooling process [36]. Moreover, m-ZrO_2 phases resulting from the stress-induced t-$ZrO_2 \rightarrow$ m-ZrO_2 phase transformation were generally found to be located along the grain boundaries [7,8]. In the same way, the large c-ZrO_2 grains around 30–40 μm and the m-ZrO_2 phases settled along the grain boundaries can play an important role in the toughness enhancement by different mechanisms e.g., crack bridging, crack deflection and crack branching [7,8]. However, the linear decrease observed in hardness due to the addition of 8 Mg-PSZ can be explained by the Hall–Pecth equation [37,38], expressing that the hardness of a material decreases with the increasing grain size. At this point, it can be considered that the hardness values of composites decrease with large c-ZrO_2 grains arising from the 8 Mg-PSZ addition.

To clarify these facts, the indent trace of 0.5(3Y-TZP)/0.5(8 Mg-PSZ) composite sample sintered at 1500°C-2h, which exhibited a significant enhancement on the mechanical properties herein, was examined in detail by SEM and EDX analyses. The obtained microstructural observations were also given in Fig. 4(a–f). At first glance in Fig. 4(a), it could be seen that while the Vickers indent trace was located in the middle of the SEM-BSE image, the characteristic crack formations occurred in the Y-TZP and Mg-PSZ regions after stress-induced. Here, please note that the polygonal-shaped c-ZrO_2 grains developed at ~3–10 μm grain size in Mg-PSZ region, whereas t-ZrO_2 grains were of submicron-size similar to spherical morphology in the 3Y-TZP region. In Fig. 4(b), the nano-sized t-ZrO_2 precipitates were determined to be formed within the c-ZrO_2 grains (indicated by black arrows). As known, these precipitates play an important role on the toughness increase in Mg-PSZ ceramics by causing t→m phase transformation under an applied stress [13,36]. Therefore, observation of spherical nano-sized m-ZrO_2 grains during transgranular cracking (Fig. 4(b)) can also be considered here as clear evidence that toughness was increased by stress-induced t-$ZrO_2 \rightarrow$ m-ZrO_2 phase transformation. More interestingly, when looking at Fig. 4(b) in detail, it was determined that the intergranular cracking proceeded around the primary large c-ZrO_2 and transformed m-ZrO_2 grains located at the grain boundaries. Thus, the energy of the crack was reduced, contributing to the increase of fracture toughness [7,8,36]. Moreover, while the crack was absorbed by the primary large c-ZrO_2 grains, the toughness enhancement mechanisms e.g. crack bridging, crack deflection and crack branching helped to reduce the total energy of the crack as well [Fig. 4(c)]. To better understand the

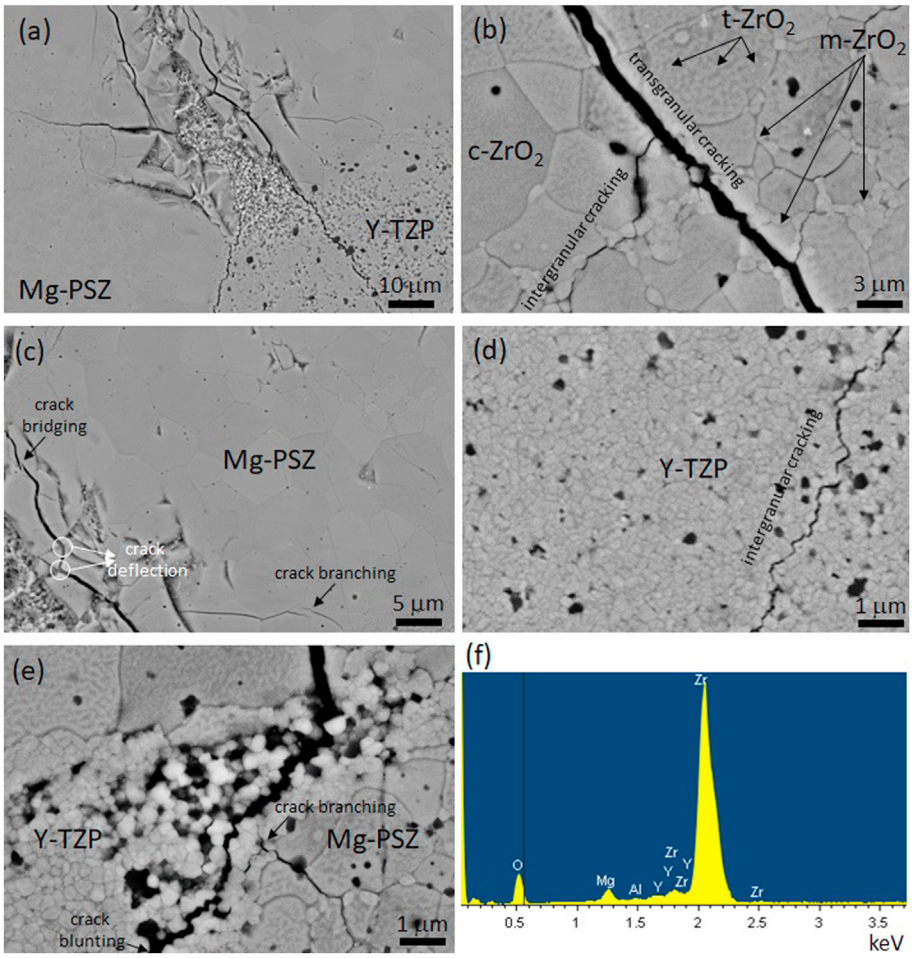

Fig. 4. SEM-BSE images visualized from 0.5(3Y-TZP)/0.5(8 Mg-PSZ) composite sintered at 1500°C-2h revealing (a) Vickers indent trace, (b) transgranular and intergranular propagating cracks in Mg-PSZ, (c) energy-absorbing mechanisms such as crack bridging, crack deflection and crack branching in Mg-PSZ, (d) intergranular cracking in YTZ, (e) mix region with Y-TZP and Mg-PSZ grains, and (f) EDX spectrum acquired from whole region in Fig. 4(e).

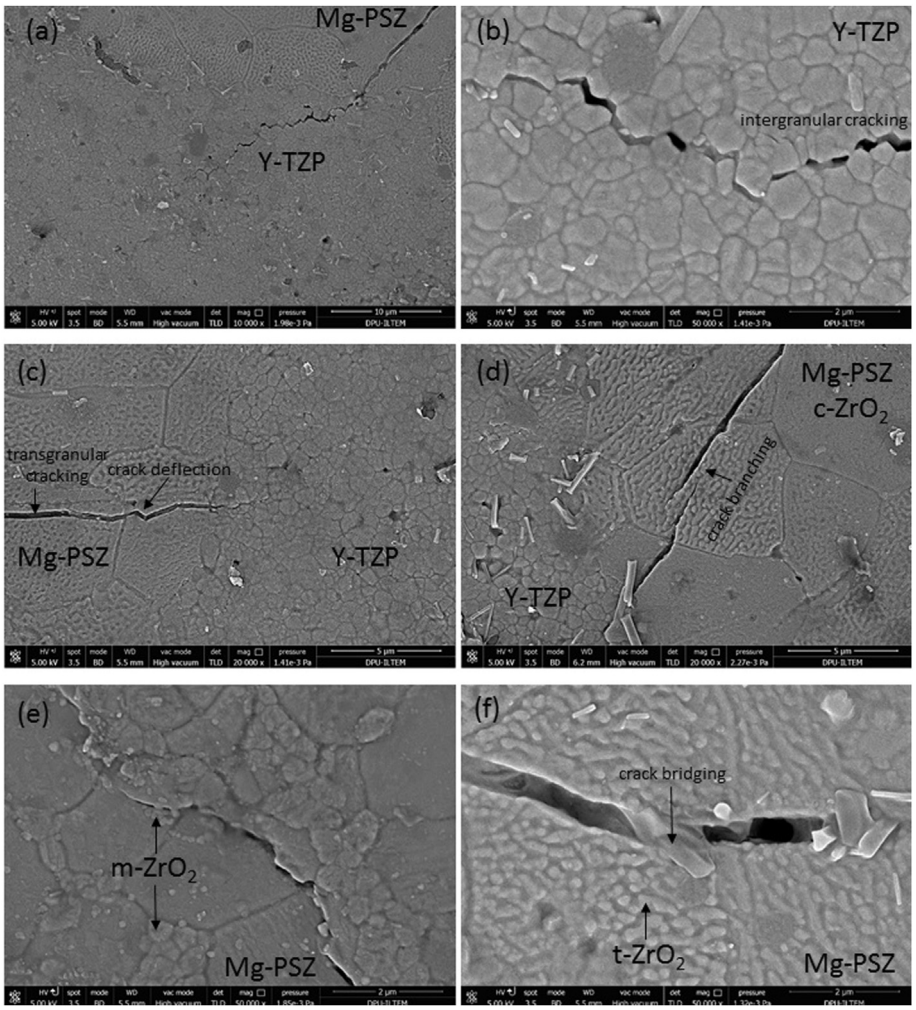

Fig. 5. (a–f) UHR-SEM/BSE images acquired from 5(3Y-TZP)/0.5(8 Mg-PSZ) composite sintered at 1500°C-2h.

impact of these mechanisms, it is necessary to analyze the SEM-BSE images given in Fig. 4(d and e). Accordingly, as the crack progressed continuously along the Y-TZP grain boundaries without encountering no further toughening mechanism rather than t→m phase transformation [Fig. 4(d)]; however, it was firstly branched and then blunted by decreasing its energy in the case of Mg-PSZ grains around it [Fig. 4(e)]. Furthermore, the detection of Y, Mg, Zr and O elements in the EDX spectrum [Fig. 4(f)] chemically confirmed coexistence of the Y-TZP and Mg-PSZ grains in Fig. 4(e). Thus, these microstructural results clearly support that why the mechanical properties given in Fig. 3(a and b) were improved when Y-TZP and Mg-PSZ were used together.

In order to get deep understanding of the facture toughness evaluation through 8 Mg-PSZ addition, the 0.5(3Y-TZP)/0.5(8 Mg-PSZ) composite sample sintered at 1500°C-2h was also characterized by using a field emission gun (FEG) ultra-high resolution scanning electron microscope (UHR-SEM). The obtained SEM-BSE images were presented in Fig. 5(a–f). Here, considering the Fig. 5(a), a crack propagation can be easily seen between the Mg-PSZ and Y-TZP regions in the composite sample. At this point, we state that the interganular cracking is characteristic for the Y-TZP region, and no further toughing mechanism excepting t→m phase transformation is available herein, as can be discerned from the Fig. 5(b). However, the transgranular cracking along the large c-ZrO_2 grains that also including intense t-ZrO_2 precipitates (marked with Mg-PSZ in [Fig. 5(c)]) drastically reduces the crack's energy. In addition, the crack deflection mechanism positively contributes to energy reduction of propagating crack until it reaches to Y-TZP region. Thus, the cracking was totally absorbed by Mg-PSZ grains before cracks did not introduce into the Y-TZP grains. Moreover, the crack branching within the c-ZrO_2 (Mg-PSZ) grains was clearly observed in Fig. 5(d), and this gave rise to similarly crack's energy reduction and/or blunting of the cracking. Furthermore, nano-size m-ZrO_2 grains along the Mg-PSZ grain boundaries due to the t→m phase transformation under the stress were detected in Fig. 5(e). This can also be considered as an alternative way to lower the crack's energy. More interestingly, for the same purpose, the crack bridging occurrence was observed in the c-ZrO_2 (Mg-PSZ) grains, which were densely composed of t-ZrO_2 grains [Fig. 5(f)]. So, all these observed microstructural features originated from Mg-PSZ addition, i.e. crack's energy reduction, crack deflection, crack branching, stress-induced t→m ZrO_2 phase transformation, and crack bridging played a key role on the improvement of fracture toughness in Y-TZP ceramics [7,8,13,36].

4. Conclusion

The fracture toughness of 3Y-TZP ceramics was enhanced by incorporating 8 Mg-PSZ powders having high toughness into the 3Y-TZP powders. As-received (3Y-TZP and 8 Mg-PSZ) and composite (x3Y-TZP/y8Mg-PSZ; where x and y vary between 25% and 75% in weight) samples were successfully densified over ~99% of relative

density at 1450°C–1500 °C for 1–2 h by using pressureless sintering method. The relative density, Vickers hardness (HV) and indentation fracture toughness (K_{Ic}) of sintered samples were improved by increasing sintering temperature and holding time. Also, the HV and K_{Ic} values of composite bodies (x3Y-TZP/y8Mg-PSZ) can be easily tailored by increasing the content of 8 Mg-PSZ. In particular, the HV and K_{Ic} values of 0.5(3Y-TZP)/0.5(8 Mg-PSZ) composite sintered at 1500 °C for 2 h increased by 7% and 30%, respectively, compared to that of 3Y-TZP as-received sample. According to XRD analysis, it was determined that sintered bodies only contained the c-ZrO_2, t-ZrO_2 and m-ZrO_2 phases without observing any new phase formation. In addition, m-ZrO_2/c-ZrO_2+t-ZrO_2 volumetric phase ratios changed with increasing sintering temperature and time. Based on the detailed SEM and EDX analyses obtained from the indent trace of composite samples, the stress-induced t-ZrO_2 → m-ZrO_2 phase transformation within c-ZrO_2 grains in 8 Mg-PSZ was determined as the main mechanism in toughness enhancement. In addition, crack-bridging, crack-deflection and crack branching mechanisms contributed to toughness increase. It is anticipated that different zirconia-based composites that not only improved toughness but also other mechanical properties can be produced for functional and structural applications by the easy, fast and practicable approach presented here.

Declaration of competing interest

The authors declare that they have no known competing financial interests or personal relationships that could have appeared to influence the work reported in this paper.

Acknowledgments

The authors wish to express their sincere gratitude to Professor Dr. Servet Turan and MSc candidate Alparslan Ali Balta (Eskişehir Technical University, Turkey) for allowing the use of SEM laboratory and mechanical test facilities as well as their contributions during the analyses. We would like to also thank the Kutahya Dumlupinar University Advanced Technologies Research Center (DPU-ILTEM) for the UHR-SEM investigations.

References

[1] J. Chevalier, L. Gremillard, Ceramics for medical applications: a picture for the next 20 years, J. Eur. Ceram. Soc. 29 (2009) 1245–1255, https://doi.org/10.1016/j.jeurceramsoc.2008.08.025.
[2] B. Basu, Toughening of yttria-stabilised tetragonal zirconia ceramics, Int. Mater. Rev. 50 (2005) 239–256, https://doi.org/10.1179/174328005X41113.
[3] A. Yurdakul, H. Gocmez, One-step hydrothermal synthesis of yttria-stabilized tetragonal zirconia polycrystalline nanopowders for blue-colored zirconia-cobalt aluminate spinel composite ceramics, Ceram. Int. 45 (2019) 5398–5406, https://doi.org/10.1016/j.ceramint.2018.11.240.
[4] I. Nettleship, R. Stevens, Tetragonal zirconia polycrystal (TZP)-a review, Int. J. High Technol. Ceram. 3 (1987) 1–32, https://doi.org/10.1016/0267-3762(87)90060-9.
[5] R.H. Hannink, P.M. Kelly, B.C. Muddle, Transformation toughening in zirconia-containing ceramics, J. Am. Ceram. Soc. 83 (3) (2000) 461–487.
[6] J.J. Swab, Low temperature degradation of Y-TZP materials, J. Mater. Sci. 26 (1991) 6706–6714, https://doi.org/10.1007/BF00553696.
[7] D.L. Porter, A.H. Heuer, Microstructural development in MgO-partially stabilized zirconia (Mg-PSZ), J. Am. Ceram. Soc. 62 (1979) 298–305, https://doi.org/10.1111/j.1151-2916.1979.tb09484.x.
[8] J.A.B. Chaparro, A.R. Rojas, M.H.B. Bernal, A.A. Elguezabal, J. Echeberria, Elucidating of the microstructure of ZrO_2 ceramics with additions of 1200°C heat treated ultrafine MgO powders: aging at 1420°C, Mater. Chem. Phys. 106 (2007) 45–53, https://doi.org/10.1016/j.matchemphys.2007.05.024.
[9] R.K. Govila, Strength characterization of MgO-partially stabilized zirconia, J. Mater. Sci. 26 (1991) 1545–1555, https://doi.org/10.1007/BF00544663.
[10] L. Jiang, S. Guo, Y. Bian, M. Zhang, W. Ding, Effect of sintering temperature on mechanical properties of magnesia partially stabilized zirconia refractory, Ceram. Int. 42 (2016) 10593–10598, https://doi.org/10.1016/j.ceramint.2016.03.136.
[11] Y. Chieko, P.J.O. Armani, Influence of Y_2O_3 addition on the microstructure and mechanical properties of Mg-PSZ ceramics, J. Mater. Sci. Eng. 1 (2011) 556–561, https://doi.org/10.17265/2161-6213/2011.09.014.
[12] Y. Kubota, M. Ashizuka, E. Ishida, T. Mitamura, Influence of temperature on elastic modulus and strength of MgO-partially stabilized zirconia (Mg-PSZ), J. Ceram. Soc. Jpn. 102 (1994) 708–712, https://doi.org/10.2109/jcersj.102.708.
[13] R.H.J. Hannink, M.V. Swain, Progress in transformation toughening of ceramics, Annu. Rev. Mater. Sci. 24 (1994) 359–408, https://doi.org/10.1146/annurev.ms.24.080194.002043.
[14] R.C. Garvie, C. Urbani, D.R. Kennedy, J.C. McNeuer, Biocompatibility of magnesia-partially stabilized zirconia (Mg-PSZ) ceramics, J. Mater. Sci. 19 (1984) 3224–3228, https://doi.org/10.1007/BF00549808.
[15] M. Trunec, Z. Chlup, Higher fracture toughness of tetragonal zirconia ceramics through nanocrystalline structure, Scripta Mater. 61 (2009) 56–59, https://doi.org/10.1016/j.scriptamat.2009.03.019.
[16] J. Zou, Y. Zhong, M. Eriksson, L. Liu, Z. Shen, Tougher zirconia nanoceramics with less yttria, Adv. Appl. Ceram. 118 (2019) 9–15, https://doi.org/10.1080/17436753.2018.1445464.
[17] Q. Jing, J. Bao, F. Ruan, X. Song, S. An, Y. Zhang, Z. Tian, H. Lv, J. Gao, M. Xie, High-fracture toughness and aging-resistance of 3Y-TZP ceramics with a low Al_2O_3 content for dental applications, Ceram. Int. 45 (2019) 6066–6073, https://doi.org/10.1016/j.ceramint.2018.12.078.
[18] W. Wu, Z. Xien, W. Xue, L. Cheng, Toughening effect of multiwall carbon nanotubes on 3Y-TZP zirconia ceramics at cryogenic temperatures, Ceram. Int. 41 (2015) 1303–1307, https://doi.org/10.1016/j.ceramint.2014.09.061.
[19] L. Shuang, X. Zhipeng, Z. Yumin, Z. Yufeng, Enhanced toughness of zirconia ceramics with graphene platelets consolidated by spark plasma sintering, Int. J. Appl. Ceram. Technol. 14 (2017) 1062–1068, https://doi.org/10.1111/ijac.12742.
[20] A. Borrell, M.D. Salvador, E. Rayon, F.L.P. Foix, Improvement of microstructural properties of 3Y-TZP materials by conventional and non-conventional sintering techniques, Ceram. Int. 38 (2012) 39–43, https://doi.org/10.1016/j.ceramint.2011.06.035.
[21] S. Rezaee, K. Ranjbar, A.R. Kiasat, Characterization and strengthening of porous alumina-20 wt% zirconia ceramic composites, Ceram. Int. 46 (2020) 893–902, https://doi.org/10.1016/j.ceramint.2019.09.047.
[22] R.F. Gibson, Principles of Composite Material Mechanics, CRC Press Taylor and Francis Group, Boca Raton, 2012.
[23] C.H. Ting, S. Ramesh, C.Y. Tan, N.I. Zainal Abidin, W.D. Teng, I. Urriés, L.T. Bang, Low-temperature sintering and prolonged holding time on the densification and properties of zirconia ceramic, J. Ceram. Process. Res. 18 (2017) 569–574.
[24] S.A. Nightingale, R.H.J. Hannink, S. Street, Science and Technology of Zirconia V, Technomic Publishing Co. Inc, Basel, 1993.
[25] H. Toraya, M. Yoshimura, S. Somiya, Calibration curve for quantitative analysis of the monoclinic-tetragonal ZrO_2 system by X-ray diffraction, J. Am. Ceram. Soc. 67 (1984) C-119–C-121, https://doi.org/10.1111/j.1151-2916.1984.tb19715.x.
[26] W. Zhang, J. Bao, G. Jia, W. Guo, X. Song, S. An, The effect of microstructure control on mechanical properties of 12Ce-TZP via two-step sintering method, J. Alloys Compd. 711 (2017) 686–692, https://doi.org/10.1016/j.jallcom.2017.04.059.
[27] K. Niihara, R. Morena, D.P.H. Hasselman, Evaluation of Kıc of brittle solids by the indentation method with low crack-to-indent ratios, J. Mater. Sci. Lett. 1 (1982) 13–16, https://doi.org/10.1007/BF00724706.
[28] K. Niihara, R. Morena, D.P.H. Hasselman, Fracture Mechanics of Ceramics, Plenum Press, New York, 1983.
[29] B.A. Cottom, M.J. Mayo, Fracture toughness of nanocrystalline ZrO_2-3mol% Y_2O_3 determined by Vickers indentation, Scripta Mater. 34 (1996) 809–814, https://doi.org/10.1016/1359-6462(95)00587-0.
[30] M.S. Kaliszewski, G. Behrens, A.H. Heuer, M.C. Shaw, D.B. Marshall, G.W. Dransmanri, R.W. Steinbrech, A. Pajares, F. Guiberteau, F.L. Cumbrera, A.D. Rodriguez, Indentation studies on Y_2O_2-stabilized ZrO_2: I, Development of indentation-induced cracks, J. Am. Ceram. Soc. 77 (1994) 1185–1193, https://doi.org/10.1111/j.1151-2916.1994.tb05391.x.
[31] W. Pabst, G. Ticha, E. Gregorova, Effective elastic properites of alumina-zirconia composite ceramics-Part 3. Calculation of elastic moduli of polycrystalline alumina and zirconia from monocrystal data, Ceram. Silik. 48 (2004) 41–48.
[32] J. Chevalier, L. Gremillard, A.V. Virkar, D.R. Clarke, The tetragonal-monoclinic transformation in zirconia: lessons learned and future trends, J. Am. Ceram. Soc. 92 (2009) 1901–1920, https://doi.org/10.1111/j.1551-2916.2009.03278.x.
[33] S.G. Rector, T. Blanton, The powder diffraction file: a quality materials characterization database, Powder Diffr. 34 (2019) 352–360, https://doi.org/10.1017/S0885715619000812.
[34] C.F. Grain, Phase relations in the ZrO_2-MgO system, J. Am. Ceram. Soc. 50 (1967) 288–290, https://doi.org/10.1111/j.1151-2916.1967.tb15111.x.
[35] C. Pascual, P. Durán, Subsolidus phase equilibria and ordering in the system ZrO_2-Y_2O_3, J. Am. Ceram. Soc. 66 (1983) 23–27, https://doi.org/10.1111/j.1151-2916.1983.tb09961.x.
[36] D. Galusek, P. Znášik, J. Majling, The influence of cold isostatic pressing on compaction and properties of Mg-PSZ ceramics, J. Mater. Sci. Lett. 18 (1999) 1347–1351, https://doi.org/10.1023/A:1006690500585.
[37] E.O. Hall, The deformation and ageing of mild steel. 3: discussion of results, Proc. Phys. Soc. B 64 (1951) 747–753, https://doi.org/10.1088/0370-1301/64/9/303.
[38] N.J. Petch, The cleavage strength of polycrystals, J. Iron. Steel Inst. 174 (1953) 25–28.